



Original research article

A novel enhancement technique for pathological microscopic image using neutrosophic similarity score scaling

A.I. Shahin^a, K.M. Amin^b, Amr A. Sharawi^c, Yanhui Guo^{d,*}^a Department of Biomedical Engineering, HTI, Egypt^b Department of Information Technology, Menoufia University, Egypt^c Department of Biomedical Engineering, Cairo University, Egypt^d Department of Computer Science, University of Illinois at Springfield, Springfield, IL, USA

ARTICLE INFO

Article history:

Received 17 May 2016

Received in revised form 15 January 2018

Accepted 7 February 2018

Keywords:

Pathological images

Color correction

Neutrosophic similarity score

Color correction

Color image quality

ABSTRACT

In 2011, Food and Drug Administration (FDA or USFDA) certified the automated cell morphology (ACM) systems for medical use in USA. The brightness, contrast and color appearance are all factors that play a major role in the diagnosis of many blood diseases. Accordingly, enhancement of pathological microscopic image (PMI) is a crucial step to increase the efficiency of computer assisted software. Some of the previous PMI enhancement methods neglected the illumination information and others used a reference image for template matching. These methods worked under strictly controlled conditions. In this paper, a robust technique is proposed for pathological images enhancement based on neutrosophic similarity score scaling. The color image is separated into three channels, and then each channel is represented in the neutrosophic domain into three subsets T, I and F. Neutrosophic similarity score (NSS) under multi-criteria are computed and used to scale the input image. The main contribution of this paper is that red, green and blue coefficients derived from the neutrosophic calculations lead directly to an adaptive pathology image enhancement and take into consideration many color image quality (IQ) parameters like illumination, contrast and color balance where it does not focus on a single IQ parameter like previous methods. In the experiments, several microscopic image quality measurements are utilized to evaluate the proposed method's performance versus the previous enhancement techniques. The experimental results demonstrate that our proposed system is promising with low complexity, adaptive with different resolution and lighting conditions. This provides the basis for automatic medical diagnosis and further processing of medical images.

© 2018 Elsevier GmbH. All rights reserved.

1. Introduction

Human visual analysis of microscopic blood samples plays an important role in the classification of many diseases. One of the PMIs is blood smear image which contain valued information about human health and disease. The cell's morphology structure is an essential feature to help the pathologist to decide the type of disease, and another one is the color appearance

* Corresponding author.

E-mail addresses: ahmed.esmail@hti.edu.eg (A.I. Shahin), k.amin@ci.menoufia.edu.eg (K.M. Amin), amrarsha@eng.cu.edu.eg (A.A. Sharawi), yguo56@uis.edu (Y. Guo).

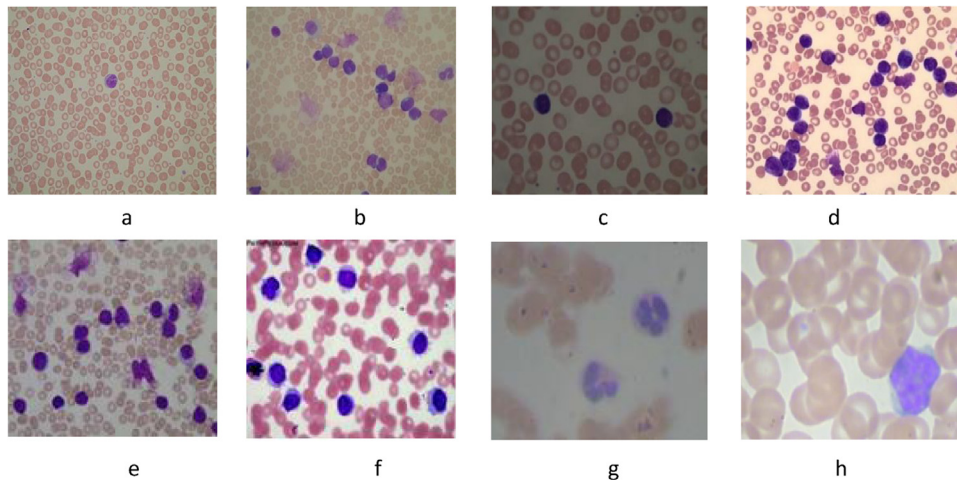


Fig. 1. Examples of degraded samples (a) low contrast image, (b) low contrast and low brightness image, (c) low brightness image, (d) good contrast good brightness, (e) good contrast low brightness, (f) good contrast good brightness, (g) low contrast and low brightness and (h) low contrast and low staining time.

of the each blood component, including red blood cells (RBCs), white blood cells (WBCs) and platelets [1]. The staining is a fundamental procedure which affects on the color appearance of each blood component [2]. After the staining procedure, the nuclei appear within cells blue and the cytoplasm appears with light blue, magenta or red according to the WBC type, which will constitutionally influence the diagnosis decision on various diseases [3]. The automated pathological imaging system (APIS) has been proved as an excellent tool in the pathological investigation and analysis. It is composed of a microscope, a charge coupled device (CCD) camera, a computer providing many operations such as digitization, storage, retrieval or viewing it on the monitor. Microscopic images are used for counting cells, analyzing shape and structure of cells and cell distribution [4].

Usually, pathological images do not have the same image quality parameters like color appearance, contrast, brightness, and resolution. This difference may be present in any procedure of APIS starting from staining and ending with imaging restoration. The difference of imaging acquisition system according to the variety of APIS in the industry will affect directly the image resolution and its quality parameters, leading to vague brightness, and low contrast, and low signal to noise ratio. Staining time also plays an important role in the contrast of the pathological image and each object intensity, as low staining time gives low sample intensity [5].

The challenge to be solved in many microscopic images is to find an adaptive preprocessing technique for each image under different conditions. In Fig. 1, different samples are collected from different datasets with different imaging conditions like resolution, contrast, brightness and background color. Fig. 1a and b have low contrast. Fig. 1c has low brightness. Fig. 1d–f are ideal images where each blood component appears at good contrast and brightness with a clear background. Fig. 1g and h have low contrast and weak cytoplasm appearance, mostly due to short staining time. There also variations between these images. In Fig. 1a, d, f and g, there are different background colors. Staining artifacts in the background are found in Fig. 1b and g. In Fig. 1c and e, different brightness in the same sample, different color contrast values. In Fig. 1h, the weak appearance of the cytoplasm is noticed compared to the cytoplasm color appearance in Fig. 1f.

Most of the published methods only worked on images under strictly controlled conditions. By contrast, in practical applications, the blood smear images to be analyzed do not always have good color consistency. Therefore, color adjustment for blood smear images is necessary [6]. Accordingly, there is a genuine need to adaptively restore degraded images from different APIS platforms.

In the pre-processing procedure of microscopic images, numerous approaches were proposed specifically for contrast enhancement. These methods include contrast adjustment by a combination of shifting of color values and linear transformation [7], nonlinear fixed transformation of the gray levels [8], and histogram stretching [9]. Moreover, histogram equalization (HE) [9], contrast limited adaptive histogram equalization (CLAHE) [10] and its modifications [11]. These techniques were popularly employed for their simplicity and good performance over a variety of images. However, they also established major changes in the pixels values and produce some distortion [12].

Other approaches were employed specifically for PMI enhancement like $\bar{r}g$ chroma [13] which was not correlated with brightness changes and neglect the illumination values. In [14], a general technique for color correction was proposed. The technique depended on CIE-Lab color space modification to correct the brightness and contrast of the image. However, this method was not robust as it needed a standard high-quality pathology image as a reference to correct the degraded one [6].

Neutrosophic set (NS) is a new general formal framework to study the neutralities, origin, nature, and scope. Any indeterminate information can be handled with its inherent ability. The neutrosophic transform (NT) has been used in many applications in image processing such as image enhancement [15], image thresholding [16], edge detection [17] and so on.

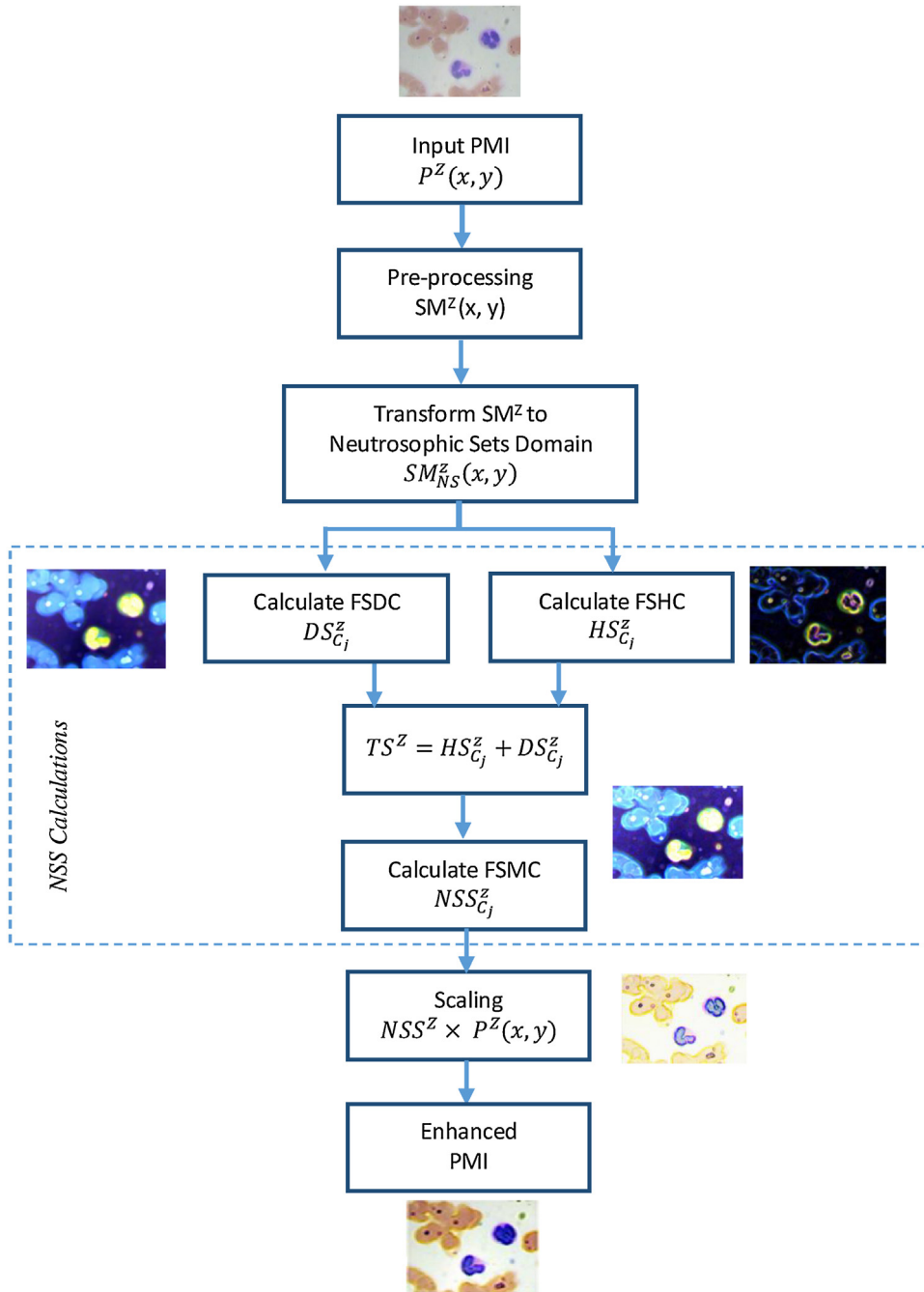


Fig. 2. The proposed system for pathological image enhancement based on NSS.

There were many previous research articles used the NT with the color image. In [18], NT was used for segmentation the color image. In [19], NT was used to enhance the clustering result of satellite image through using LUV color space. Satellite color images were transformed to LUV color space, and NT was applied to each channel of LUV color space, then a reverse transform to RGB color space was applied to get the processed image.

In this paper, a first application for the color image enhancement using neutrosophic set similarity score (NSS) is proposed. The NSS is utilized to extract the enhanced RGB coefficients where each channel coefficients are calculated separately. Then, the resultant coefficients are utilized to scale the input image. This scaling has an obvious enhancement effect on image quality parameters which is proved experimentally.

The rest of the paper is organized as follows: in the next sections, we present the related work on neutrosophic sets and its applications, then the proposed method of PMI enhancement is discussed in details. Finally, the experimental results followed by the conclusion section in the reminder of the paper.

2. Related work

An image was defined in the neutrosophic set (NS) [15] as: let U be a universe, BP be a bright pixel set in U , and an image I_m described using NS is called neutrosophic image I_{NS} . The neutrosophic image I_{NS} is interpreted using subsets T, I and F . A pixel in I_{NS} is denoted as $P_{NS}(T, I, F)$, and it belongs to the bright pixel set BP in the means as: it is T true in the bright pixel set, I indeterminate, and F false. The range of the values in T, I, F is in $[0, 1]$.

According to the definition of the neutrosophic image, a pixel $P(x, y)$ is interpreted in the neutrosophic set domain: $P_{NS}(x, y) = \{T(x, y), I(x, y), F(x, y)\}$. $T(x, y), I(x, y)$ and $F(x, y)$ represent memberships belonging to bright pixel set, indeterminate set and non-bright pixel set, respectively. At the intensity criterion, they are defined as:

$$T_{C_g}(x, y) = \frac{g(x, y) - g_{\min}}{g_{\max} - g_{\min}} \tag{1}$$

$$I_{C_g}(x, y) = 1 - \frac{Gd(i, j) - Gd_{\min}}{Gd_{\max} - Gd_{\min}} \tag{2}$$

$$F_{C_g}(x, y) = 1 - T_{C_g}(x, y) \tag{3}$$

Where $g(x, y)$ is the gray level or intensity of the gray scale image value at the position of (x, y) on the image and $Gd(x, y)$ is the gradient magnitude value on the gray scale image at the position of (x, y) on the image.

NSS is defined by [20] to measure the similarity degree between different elements, and has been applied widely in image processing as mentioned before due to its ability to describe the indeterminate information such as noises and vague boundary in images. A neutrosophic set can be defined as [21]: let $A = \{A_1, A_2, \dots, A_m\}$ be a set of alternatives in neutrosophic set, and $C = \{C_1, C_2, \dots, C_n\}$ be a set of criteria. The alternative A_i at C_j criterion is denoted as $\{T_{C_j}(A_i), I_{C_j}(A_i), F_{C_j}(A_i)\} / A_i$, where $T_{C_j}(A_i), I_{C_j}(A_i)$ and $F_{C_j}(A_i)$ are the membership values to the true, indeterminate and false set at the C_j criterion.

The similarity measurement is employed to measure the similarity between two elements in neutrosophic set under multi-criteria as [16]:-

$$S_{C_j}(A_m, A_n) = \frac{T_{C_j}(A_m)T_{C_j}(A_n) + I_{C_j}(A_m)I_{C_j}(A_n) + F_{C_j}(A_m)F_{C_j}(A_n)}{\sqrt{T_{C_j}^2(A_m) + I_{C_j}^2(A_m) + F_{C_j}^2(A_m)}\sqrt{T_{C_j}^2(A_n) + I_{C_j}^2(A_n) + F_{C_j}^2(A_n)}} \tag{4}$$

In a multi-criteria environment, the concept of the ideal element can be used to identify the best alternative. The ideal alternative A^* is denoted as: $\{T_{C_j}^*(A_i), I_{C_j}^*(A_i), F_{C_j}^*(A_i)\} / A_i^*$. The similarity to the ideal alternative is calculated as:

$$S_{C_j}(A_i, A^*) = \frac{T_{C_j}(A_i)T_{C_j}(A^*) + I_{C_j}(A_i)I_{C_j}(A^*) + F_{C_j}(A_i)F_{C_j}(A^*)}{\sqrt{T_{C_j}^2(A_i) + I_{C_j}^2(A_i) + F_{C_j}^2(A_i)}\sqrt{T_{C_j}^2(A^*) + I_{C_j}^2(A^*) + F_{C_j}^2(A^*)}} \tag{5}$$

In [20], the weighted correlation coefficients $w_k = [w_1, w_2 \dots w_n]$ were used to take the weights of each element into consideration:

$$S_{C_j}(A_i, A^*) = \frac{w_k [T_{C_j}(A_i)T_{C_j}(A^*) + I_{C_j}(A_i)I_{C_j}(A^*) + F_{C_j}(A_i)F_{C_j}(A^*)]}{\sqrt{w_k(T_{C_j}^2(A_i) + I_{C_j}^2(A_i) + F_{C_j}^2(A_i))}\sqrt{w_k(T_{C_j}^2(A^*) + I_{C_j}^2(A^*) + F_{C_j}^2(A^*))}} \tag{6}$$

For a pixel $P(x, y)$, the similarity score is calculated to identify the degree to the ideal object for a gray scale intensity image.

$$S_{C_j}(P(x, y), A^*) = \frac{w_k [T_{C_j}(x, y)T_{C_j}(A^*) + I_{C_j}(x, y)I_{C_j}(A^*) + F_{C_j}(x, y)F_{C_j}(A^*)]}{\sqrt{w_k(T_{C_j}^2(x, y) + I_{C_j}^2(x, y) + F_{C_j}^2(x, y))}\sqrt{w_k(T_{C_j}^2(A^*) + I_{C_j}^2(A^*) + F_{C_j}^2(A^*))}} \tag{7}$$

3. Proposed technique

In this section, a novel algorithm based on NSS is proposed to enhance PMI by computing scale coefficients NSS^2 . The algorithm not only improves contrast, brightness of the input image but also adjust differential color appearance difference for different blood components. The proposed algorithm consists of four main stages: pre-processing, transformation to the neutrosophic sets domain, NSS calculations and scaling as (shown in Fig. 2).

3.1. Pre-processing

The pre-processing stage is implemented by applying a smoothing filter to each color channel. We apply an averaging filter with a disk element whose radius $r = 5$ pixels, with a square averaging kernel of size $E = (2*r + 1)$. The filter size is minimized to overcome the interference between cytoplasm and the background in the pathological image, and also prevent blurring effect. This smoothing stage is important in the NSS calculations according to their sensitivity to noisy pixels as reported by [16]. For a color image P^z with size (x,y) where z is referred to any of three color channel $z = \{\text{red, green or blue}\}$, the smoothed image is defined as SM^z with size (x,y) .

3.2. Transformation to neutrosophic sets domain

For a smoothed color image pixel $SM^z(x, y)$, the neutrosophic sets ($T_{C_j}^z(x, y)$, $I_{C_j}^z(x, y)$ and $F_{C_j}^z(x, y)$) can be interpreted for each color channel at specific pixel $SM_{NS}^z(x, y)$ where each channel z has its own neutrosophic sets for each pixel value (x,y) at a specific criteria j . Then, the processed channels are concatenated again in a single color image as in [19] for any further processing.

3.3. NSS calculations

In our system, three-stages of NSS calculations are performed using different alternatives criteria and weights. The NSS algorithm is performed at multi-criteria which are the intensity criteria, local mean intensity criteria and homogeneity criteria [16], for three neutrosophic sets which are Truth, False and indeterminacy. The weights are adjusted to extract the ideal alternative at specific criteria.

3.3.1. False set at homogeneity criteria (FSHC)

For ideal alternative $A = [0\ 0\ 1]$, we extract the neutrosophic false at homogeneity criteria. We get the homogeneity criteria by adjusting the weights coefficients w_{k1} values with $[0\ 0\ 1]$. Each channel of the smoothed color image pixel $SM^z(x, y)$ has its own three neutrosophic sets for each criteria ($T_{C_j(x,y)}^z$, $I_{C_j(x,y)}^z$ and $F_{C_j(x,y)}^z$). For these alternatives and criteria, the similarity measure for false set at homogeneity criteria can be defined as:

$$HS_{C_j}^z((SM^z(x, y), A^*)) = \frac{w_{k1} [T_{C_j}^z(x, y)T_{C_j}(A^*) + I_{C_j}^z(x, y)I_{C_j}(A^*) + F_{C_j}^z(x, y)F_{C_j}(A^*)]}{\sqrt{w_{k1} (T_{C_j}^z(x, y)^2 + I_{C_j}^z(x, y)^2 + F_{C_j}^z(x, y)^2)} \sqrt{w_{k1} (T_{C_j}^2(A^*) + I_{C_j}^2(A^*) + F_{C_j}^2(A^*))}} \quad (8)$$

3.3.2. False set at dual criteria (FSDC)

For ideal Alternative $A = [0\ 0\ 1]$, we extract the neutrosophic false at dual criteria. We get the dual criteria by adjust the weights coefficients w_{k2} values with $[1\ 0\ 1]$. Each channel of the smoothed color image pixel $SM^z(x, y)$ will have its own three neutrosophic sets for each criteria ($T_{C_j(x,y)}^z$, $I_{C_j}^z(x, y)$ and $F_{C_j}^z(x, y)$). For these alternatives and criteria, the similarity measure for the false set at only dual criteria.

$$DS_{C_j}^z((SM^z(x, y), A^*)) = \frac{w_{k2} [T_{C_j}^z(x, y)T_{C_j}(A^*) + I_{C_j}^z(x, y)I_{C_j}(A^*) + F_{C_j}^z(x, y)F_{C_j}(A^*)]}{\sqrt{w_{k2} (T_{C_j}^z(x, y)^2 + I_{C_j}^z(x, y)^2 + F_{C_j}^z(x, y)^2)} \sqrt{w_{k2} (T_{C_j}^2(A^*) + I_{C_j}^2(A^*) + F_{C_j}^2(A^*))}} \quad (9)$$

The final NSS domain (TS^z) can be obtained by adding the NSS values for each color channel for both $HS_{C_j}^z$ and $DS_{C_j}^z$ similarity values. NSS domain is highlighted edges and object together.

$$TS^z = HS_{C_j}^z + DS_{C_j}^z \quad (10)$$

3.3.3. False set at multi criteria (FSMC)

The previous NSS values were studied in the false set which overcome the change in image brightness intensity. To recover the values in the truth set (RGB color space), we calculate the false set again with ideal alternative $A = [0\ 0\ 1]$ and extract the neutrosophic false set at multi criteria (FSMC). We obtain the multi criteria by adjusting the weights coefficients w_{k3} with the best-achieved values through the experiments $[0.9\ 0.4\ 0.1]$. Each channel of the neutrosophic color image pixel $TS^z(x, y)$ will have its own three neutrosophic sets for each criterion ($T_{C_j}^z(x, y)$, $I_{C_j}^z(x, y)$ and $F_{C_j}^z(x, y)$). For these alternatives and criteria, the similarity measure for the false set weighted adjusted multi-criteria can be defined as:-

$$NSS_{C_j}^z((TS^z(x, y), A^*)) = \frac{w_{k3} [T_{C_j}^z(x, y)T_{C_j}(A^*) + I_{C_j}^z(x, y)I_{C_j}(A^*) + F_{C_j}^z(x, y)F_{C_j}(A^*)]}{\sqrt{w_{k3} (T_{C_j}^z(x, y)^2 + I_{C_j}^z(x, y)^2 + F_{C_j}^z(x, y)^2)} \sqrt{w_{k3} (T_{C_j}^2(A^*) + I_{C_j}^2(A^*) + F_{C_j}^2(A^*))}} \quad (11)$$

Table 1
Pathology images used datasets.

| | ALL.DB1 [23] | ALL.DB2 [23] | BS.DB3 [27] |
|--------------|--|--|--------------------------------------|
| Institution | Department of Information Technology - Università degli Studi di Milano, Italy | Department of Information Technology - Università degli Studi di Milano, Italy | SmartLabs Ltd., Calgary, AB, Canada. |
| Resolution | 2529 × 1944 | 257 × 257 | 640 × 480 |
| File Format | jpg | tif | bmp |
| Total Images | 108 | 260 | 2959 |

3.4. NSS scaling

Finally, we utilize the resultant NSS coefficients NSS^Z to scale the input image pixel $P^Z(x, y)$. The final enhanced image (I_{En}) is reconstructed from the output of each channel as:

$$I_{En} = NSS^Z(x, y) \times P^Z(x, y) \quad (12)$$

This method enhances the color difference, contrast and brightness in the input pathological image without producing any distortion. The advantage of this scaling that the background brightness is adjusted where the RBCs and WBCs have a correct color appearance, this obvious color difference will enhance each blood component and the overall appearance of the blood smear image.

4. Experimental results

In this section, we will discuss the experimental results. The experiments are taken on a platform with Intel® core™ i5-3210 @2.50 GHZ with 4 GB Ram and the algorithm is implemented using the software of Matlab 2016a.

4.1. Datasets

The experiments were performed using different blood smear image datasets. The total number of images is 3327. These images have different resolutions, contrasts, illuminations, and are extracted from different sources as summarized in (Table 1). In BS.DB3, a CCD camera is applied to the microscope, and the microscope magnification is adjusted at 100x objective lens. The images are acquired with 640 × 480 pixels. In ALL.DB1 and ALL.DB2, images were captured with an optical laboratory microscope coupled with a Canon PowerShot G5 camera. All images are saved in JPG and TIFF format with 24 bit color depth. The images are acquired with 2592 × 1944 pixels. The microscope magnification range is from 300 to 500 X objective lens.

All these databases are widely used in many researches before like [13,22–26]. The images in these datasets contain different types of WBCs (Basophil, Eosinophil, Lymphocyte, Monocyte and Neutrophil).

4.2. Quality metrics

Generally, there are a lot of image quality assessment (IQA) metrics have been developed to measure the color and gray image quality after enhancement. Some of them do not consider the human visual system (HVS) like mean square error (MSE) [28], Peak-signal-to-noise-ratio (PSNR) [29] and absolute mean brightness error (ABME) [30]. Others take into consideration the HVS like structural similarity index (SSIM), multi-scale structural similarity index (MSSIM), visual information fidelity (VIF) [31]. In microscopic hist-pathology images, the contrast and brightness quality metrics are very important to quantify the image quality. In [32], authors used light distortion (LD) and contrast feature which was calculated from gray level co-occurrence matrix (GLCM). The paper [33] utilized the contrast enhancement index (CII) and entropy to measure the quality after enhancement. However, the pathology images' qualities depend on how each blood component color is separated from the others. For such purpose, the color separation metric (CSM) and color difference metric (ΔE) were proposed in [34,35] in order to accurately measure how the color appearance differs between each blood component in the pathology image.

In this paper, we employ the ABME, LD, MS-SSIM, CII and ΔE as evaluation metrics which are described below.

4.2.1. Absolute mean brightness error

Absolute mean brightness error (AMBE) is mostly used to evaluate brightness preservation in processed image after image contrast enhancement, which is defined in [36] as:

$$ABME = |Xm - Ym| \quad (13)$$

where Xm is mean values of the input image and Ym is mean values of the output image. Such error should be minimized to get high quality images.

4.2.2. Luminance distortion

Luminance distortion (LD) is a measure of closeness of the mean luminance of two images being compared. For a reference image (F) and test image (G) of size(x, y). μ_F is the mean brightness of F and μ_G is the mean brightness of G, the LD is defined as :-

$$LD = \frac{2\mu_F \mu_G}{\mu_F^2 + \mu_G^2} \quad (14)$$

The LQLD value for a contrast enhanced output image is computed as a mean of the local LD values computed at its every pixel location considering the 7×7 neighborhood surrounding it. The formula for computation of the image Q is given by;

$$LQLD = \frac{1}{x * y} \sum_{i=0}^{x-1} \sum_{j=0}^{y-1} LD \quad (15)$$

4.2.3. Multi-scale structural similarity index

The structural similarity index (SSI) is a method for measuring the similarity between two images. The SSIM index is a full reference metric, in other words, the measuring of image quality based on an initial uncompressed or distortion-free image as reference. The SSIM algorithm is considered a single-scale approach that achieves its best performance when applied at an appropriate scale. Moreover, choosing the right scale depends on the viewing conditions, e.g., viewing distance and the resolution of the display. Therefore, this algorithm lacks the ability to adapt to these conditions. This drawback of the SSIM algorithm motivated researchers to design a multi-scale structural similarity index (MS-SSIM) which is given by;

$$MS - SSIM(I_{ref}, I_{tst}) = [l_{Ms}(I_{ref}, I_{tst})]^{\alpha_{Ms}} \cdot \prod_{i=1}^{Ms} [C_i(I_{ref}, I_{tst})]^{\beta_i} [S_i(I_{ref}, I_{tst})]^{\gamma_i} \quad (16)$$

where $C_i(I_{ref}, I_{tst})$ and $S_i(I_{ref}, I_{tst})$ are the contrast and the structure comparison function at the i-th scale respectively, and $l_{Ms}(I_{ref}, I_{tst})$ is the luminance comparison function at the Ms-th scale. Moreover, α_{Ms} , β_i and γ_i are positive constants chosen to indicate the relative importance of each component.

4.2.4. Contrast enhancement index

Contrast Enhancement Index (CII) is calculated as follows:-

$$CII = \frac{C_{processed}}{C_{original}} \quad (17)$$

where $C_{processed}$ is the average of all 3×3 small images contrast of enhanced images and $C_{original}$ is the average of the corresponding original images. The image (color image needs to be converted to a grayscale image) is divided into 3×3 window. The contrast of each window is calculated as follows:-

$$C = \frac{\max - \min}{\max + \min} \quad (18)$$

where the max and min are the maximum and minimum value, respectively, which is calculated from small local window.

4.2.5. Color difference metric

Color difference (ΔE) is a single number representing the Euclidean distance between two colors. As the stained samples generates a two component colors, the red blood cells (RBCs) appear in red to brown color and WBCs and platelets appear in blue to magenta color. ΔE measures the divergence between the blue and brown colors in the Pathology images. Many assumptions have been proposed to calculate ΔE as CIE76, CIE94 and CIEDE2000 standards. Because that, the rgb is intended for convenient use with electronic systems, however it doesn't align with how we actually perceive color. The CIE-LAB color space which is used to measure the color difference distance as it's the most color model actually model how the eye perceive the different colors. Using the formula in (Eq. (19)), we can extract ΔE as CIE76 standard:-

$$\Delta E_{ab} = \sqrt{(L_2 - L_1)^2 + (a_2 - a_1)^2 + (b_2 - b_1)^2} \quad (19)$$

where L_2 : is the L-channel of the whole image and L_1 : is the L-channel of the WBC region, a_2 : is the a-channel of the whole image and a_1 : is the a-channel of the WBC region and b_2 : is the b-channel of the whole image and b_1 : is the b-channel of the WBC region as (shown in Fig. 3).

4.3. Evaluation results

We perform the experiments based on different four criteria; qualitative results based on visual enhancement results of different samples of images, quantitative enhancement results, cost time results and the segmentation results based on how our proposed method increases the efficiency of the segmentation algorithm.

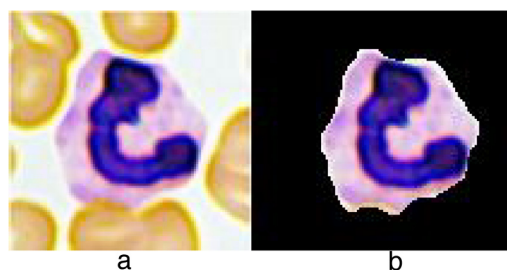


Fig. 3. (a) The whole image, (b) the WBC region.

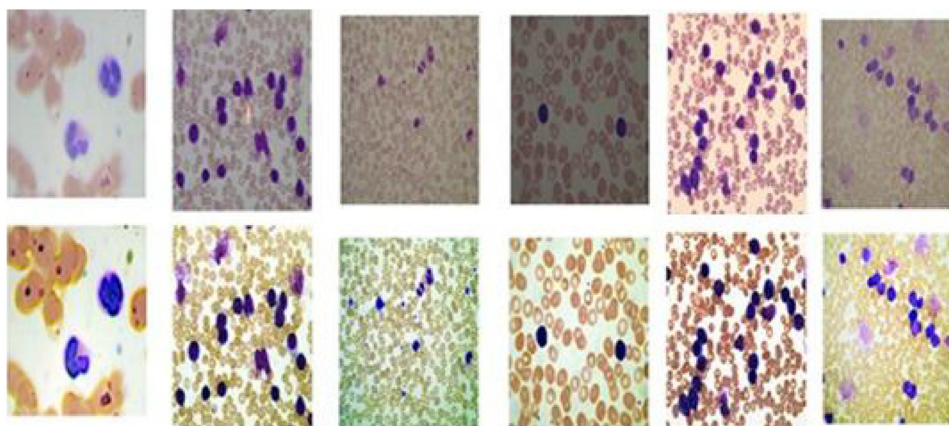


Fig. 4. (Upper) input image, (lower) Enhanced image after using our proposed system.

4.3.1. Qualitative results

In Fig. 4 (upper) a set of PMIs are selected which having low image quality parameters like poor illumination, contrast, color difference. In Fig. 4 (lower) represent the output images after NSS coefficients scaling. The proposed system is adaptive with different changes in illumination or contrast or even the resolution. The color difference between the input image and output image can be observed.

In this section, the images in Fig. 5 represent samples of experiments. The original image is shown in Fig. 5a while Fig. 5b–e represent the results obtained from previous techniques for PMI enhancement and the result of proposed technique is shown in Fig. 5f. When HE and AHE methods are used as shown in Fig. 5b and c, a distorted image is produced. On the other side, when rg chroma method is employed as shown in Fig. 5d, a low brightness image is produced. In LC method, the image histogram matching implemented with standard image, this leads to a non-robust method and does not correct the luminance as shown in Fig. 5e.

The main target for the PMI enhancement is to accurately separate the blood component visually and solve the interference between the cytoplasm and the background. The RBCs have reddish-brown color due to the appearance of hemoglobin where WBCs have a light blue cytoplasm with blue to magenta nucleus. Our proposed method using NSS in Fig. 5f appears to be the best color appearance image. In [37], the nucleus color is clearly blue where the cytoplasm color appears magenta to light blue. The RBCs color is tending to brown where the background is white and no distortion happen in it.

Previously, the enhancement techniques in PMI neglected the appearance and the distortion happened to the image as shown in Fig. 5b and c. The other previous methods enhanced a single image quality parameter as shown in Fig. 5d and e and neglect the other image quality parameters. In our proposed method shown in Fig. 5f, the image quality parameters are enhanced equally that not produce a distorting image.

4.3.2. Quantitative results

In this section, we demonstrate the performance of the proposed method in comparison with some existing PMI enhancement techniques like (He, AHE, rg chroma and LC). For LC technique, as followed in [6], standard template image that can be segmented accurately is chosen. Moreover, we choose the standard template image which achieve the best image quality evaluation parameters which we employed in our experiments. In Fig. 6, the ABME is used for different methods. The value of ABME achieved by the proposed method is very small (equals 0.014). The ABME value achieved by AHE method reach to 0.2206 (i.e. 15 times the proposed method value). For rg chroma method, ABME is 0.158 (i.e. 11.2 times the proposed method value). The HE method and LC method reflect the worst results according to their ABME values.

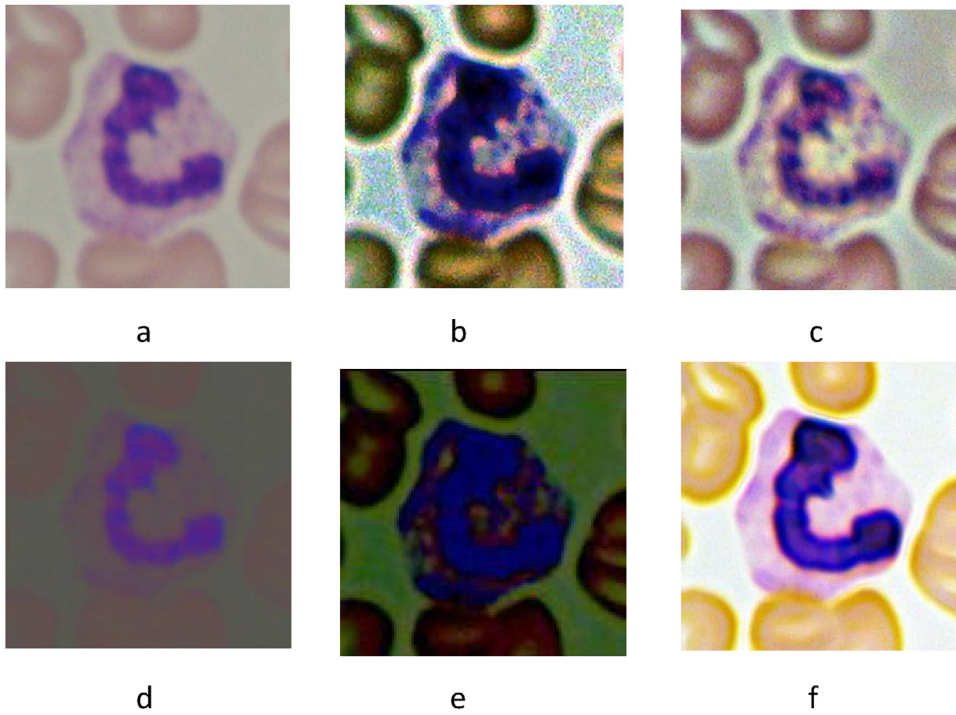


Fig. 5. (a) The original image, (b) the output of HE, (c) the output of AHE, (d) the output of rg chroma, (e) the output of LC, (f) the output of proposed system.

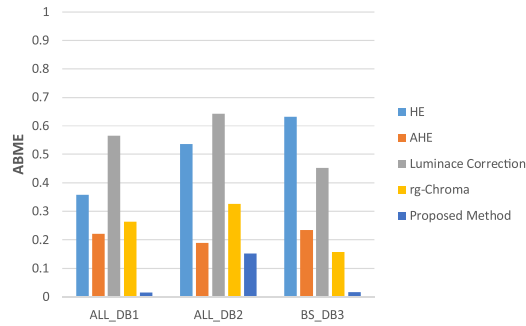


Fig. 6. Comparison of the ABME values for different datasets using different methods.

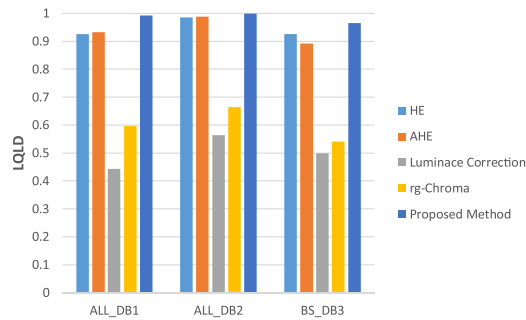


Fig. 7. Comparison between our proposed technique and previous techniques using ALL.DB1, ALL.DB2 and BS.DB3 datasets for LQLD value.

In Fig. 7, the greater the LQLD, the better the image quality is. LQLD of the proposed method has the greatest value (equal 0.999). The LQLD values which are achieved by HE and AHE methods are follow our proposed method. The rg chroma and LC method reflect the worst score values of LQLD.

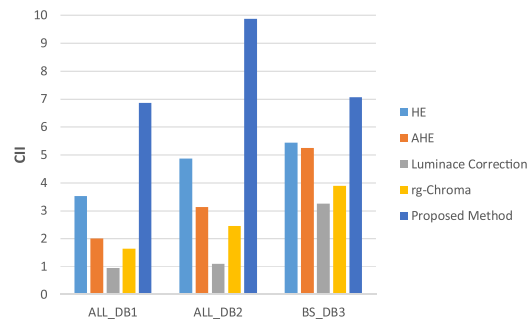


Fig. 8. Comparison between our proposed technique and previous techniques using ALL.DB1, ALL.DB2 and BS.DB3 databases for CII value.

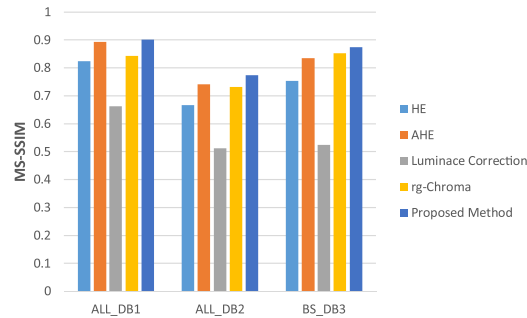


Fig. 9. Comparison between our proposed technique and previous techniques using ALL.DB1, ALL.DB2 and BS.DB3 datasets for MS-SSIM value.

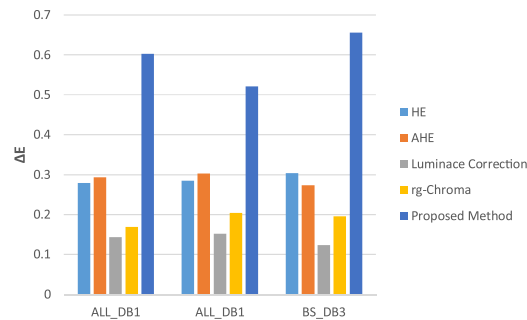


Fig. 10. Comparison between Our proposed technique and previous techniques using ALL.DB1, ALL.DB2 and BS.DB3 datasets for ΔE value.

In Fig. 8, the greater the CII, the better the image quality is. CII of proposed NSS method is the greater value equal 9.8663 where the HE and AHE are the closet values to our proposed method with a little deviation. The rg chroma and LC method reflect the worst score values of CII.

In Fig. 9, the greater the MS-SSIM, the better the image quality is. MS-SSIM of NSS is the greater value with value equal 0.990. The MS-SSIM is calculated for each color channel then the average value is calculated. The AHE and rg chroma are the closet value to our proposed method where the HE method follow them. The LC method achieved the worst MS-SSIM value.

The ΔE metric plays an important role to provide how the enhancement affects visually in color correction values. This help to easily separate the pixels between the WBCs which are stained and other non-stained blood components. In Fig. 10, the greater the ΔE , the better the image quality is. ΔE of proposed NSS method is the greater value with value equal 0.655. The AHE and HE methods achieved lower values with respect to our proposed method. Our method gives larger ΔE values with about two times their values. The rg chroma and LC methods achieved the worst ΔE value.

4.3.3. Cost time results

The performance of the different enhancement algorithms was compared based on the processing time of each algorithm as shown in Table 2. Rg-chroma method achieves the low processing time with taking into consideration that it achieved mostly the lowest performance in the previous evaluation parameters. On the other hand, the LC method consumes the highest processing time which can be explained by the required color space transformation to implement the LC algorithm. Our proposed method besides AHE and HE methods consumes an intermediate processing time. It's noticed that the processing time of our proposed method increases with the image resolution variation from 0.276 s to 0.96 s.

Table 2

A comparison of the cost time for different images resolutions using different methods.

| Dataset | Image Resolution | Cost Time (Sec per image) | | | | |
|----------|------------------|---------------------------|-------|-------|-----------------|--------------------------|
| | | rg-Chroma | HE | AHE | Proposed Method | LuminanceCorrection (LC) |
| BS.DB3 | 640 × 480 | 0.029 | 0.048 | 0.121 | 0.960 | 1.370 |
| All.IDB1 | 2529 × 1944 | 0.051 | 0.076 | 0.386 | 2.251 | 3.227 |
| All.IDB2 | 257 × 257 | 0.014 | 0.023 | 0.098 | 0.276 | 0.327 |

4.3.4. Segmentation results

To evaluate the performance of our proposed enhancement method for increasing the efficiency of segmentation algorithms in separation of different blood components in the blood smear images. We employ the k-means clustering [6] algorithm in separation of the blood smear images. The input image is transferred into HSV color space as followed in [6], then the k-mean clustering algorithm is applied to H and S color components of the input image. In Fig. 11, we perform the k-means clustering before and after applying our proposed enhancement method for six samples of blood smear images. In

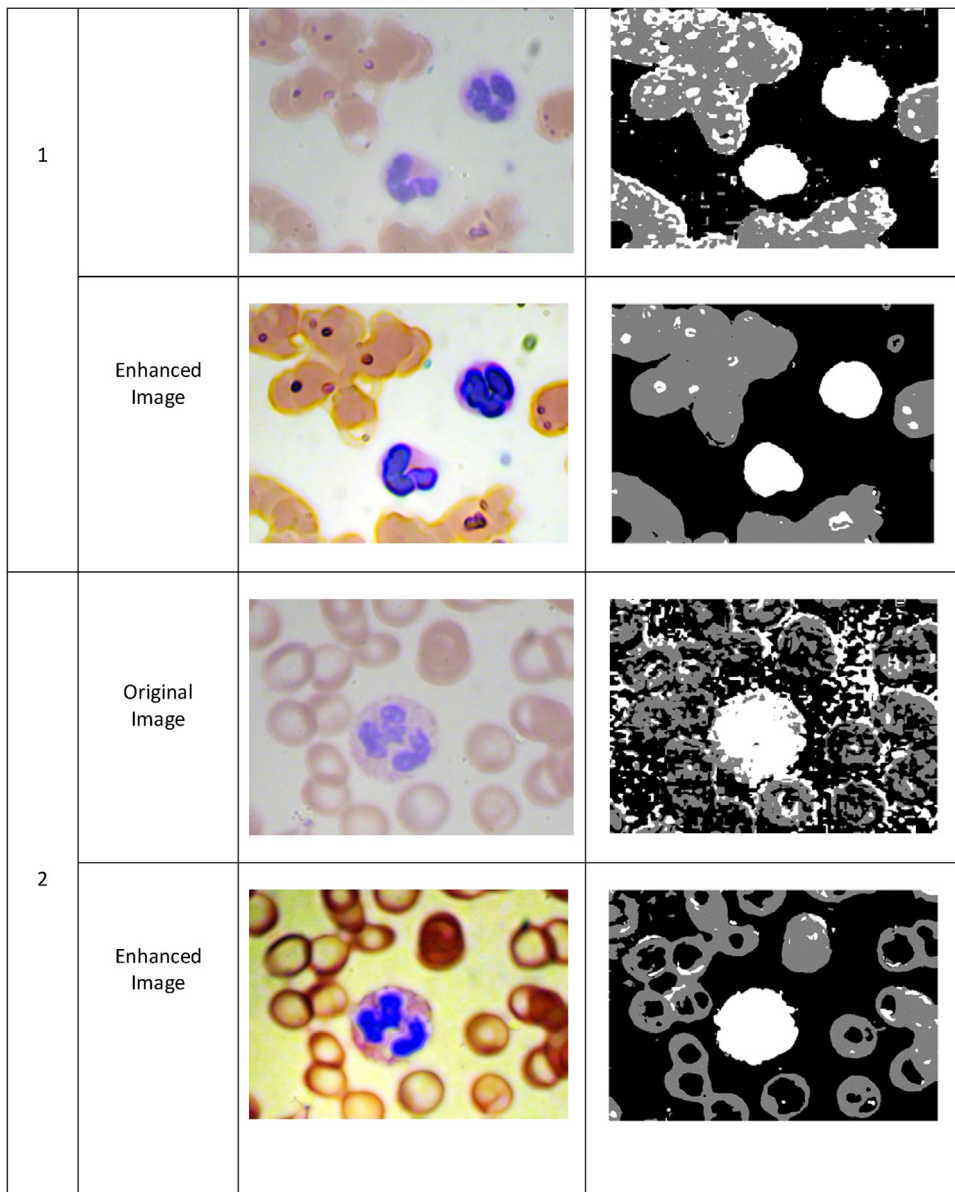


Fig. 11. The effect of our proposed enhancement method to increase the efficiency of k-means clustering algorithm in blood component separation.

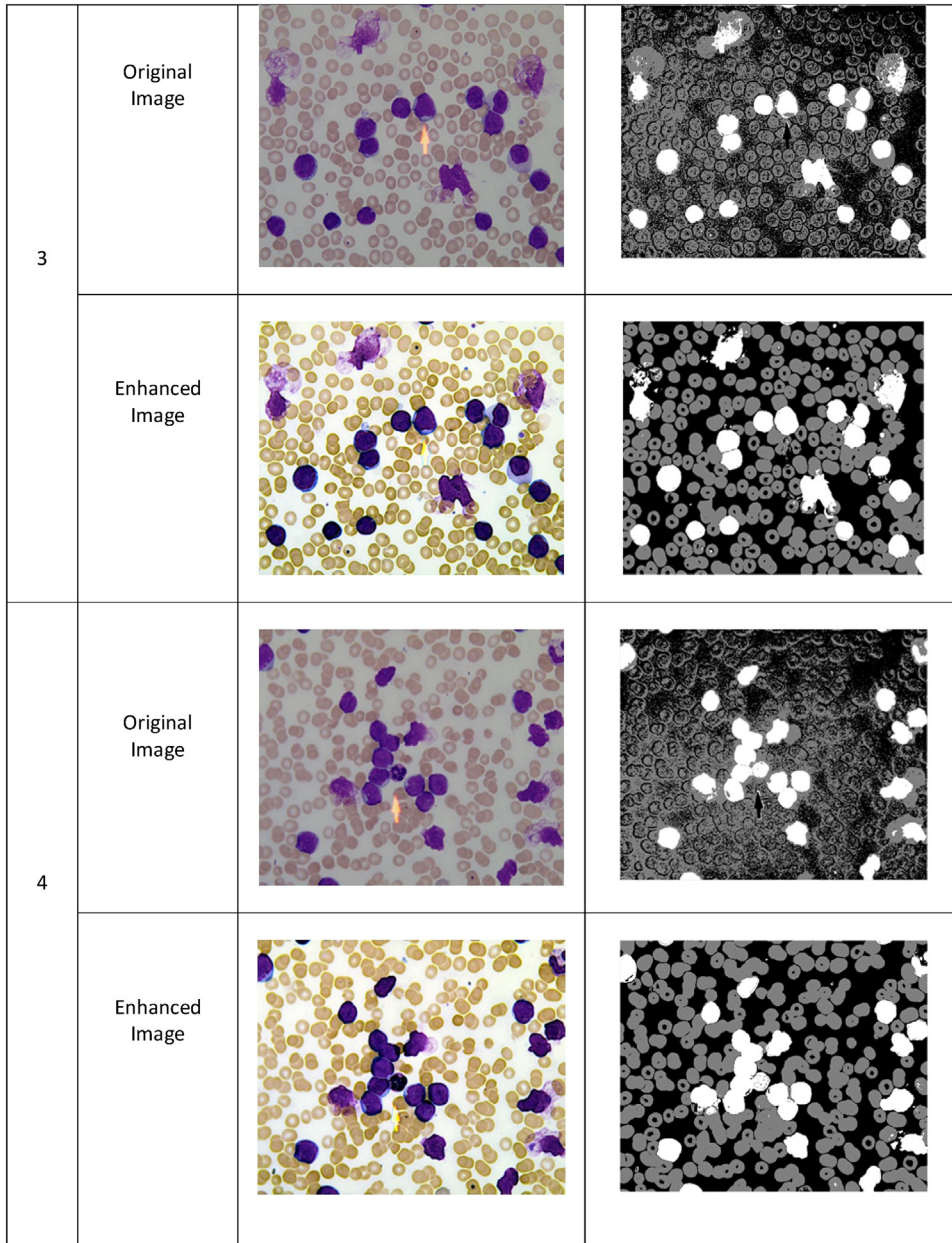


Fig. 11. (Continued)

Fig. 11, the clustered images represent the output result from the k-means clustering of the input image, RBCs are annotated by gray color, WBCs and platelets are annotated by white color, and background is annotated by black color. From the visual results of the clustering algorithm, it is noticed that our proposed enhancement method increases the performance of the segmentation algorithm by decreasing the image distortion as in sample images 1–4, and recover the missed components as in sample images 5 and 6.

5. Conclusion

This paper presents a comparative study of different pathology image enhancement techniques. It appears to be a novel and efficient technique for brightness, contrast, and color appearance enhancement to utilize NSS in pathology color images enhancement. Our proposed method does not depend on other standard color space transformation like CIE-lab or enhancing a single IQ parameter with neglecting the others. The proposed enhanced image does not contain any background distortion. An obvious color difference between each blood component is visually observed, and it will make the segmentation step

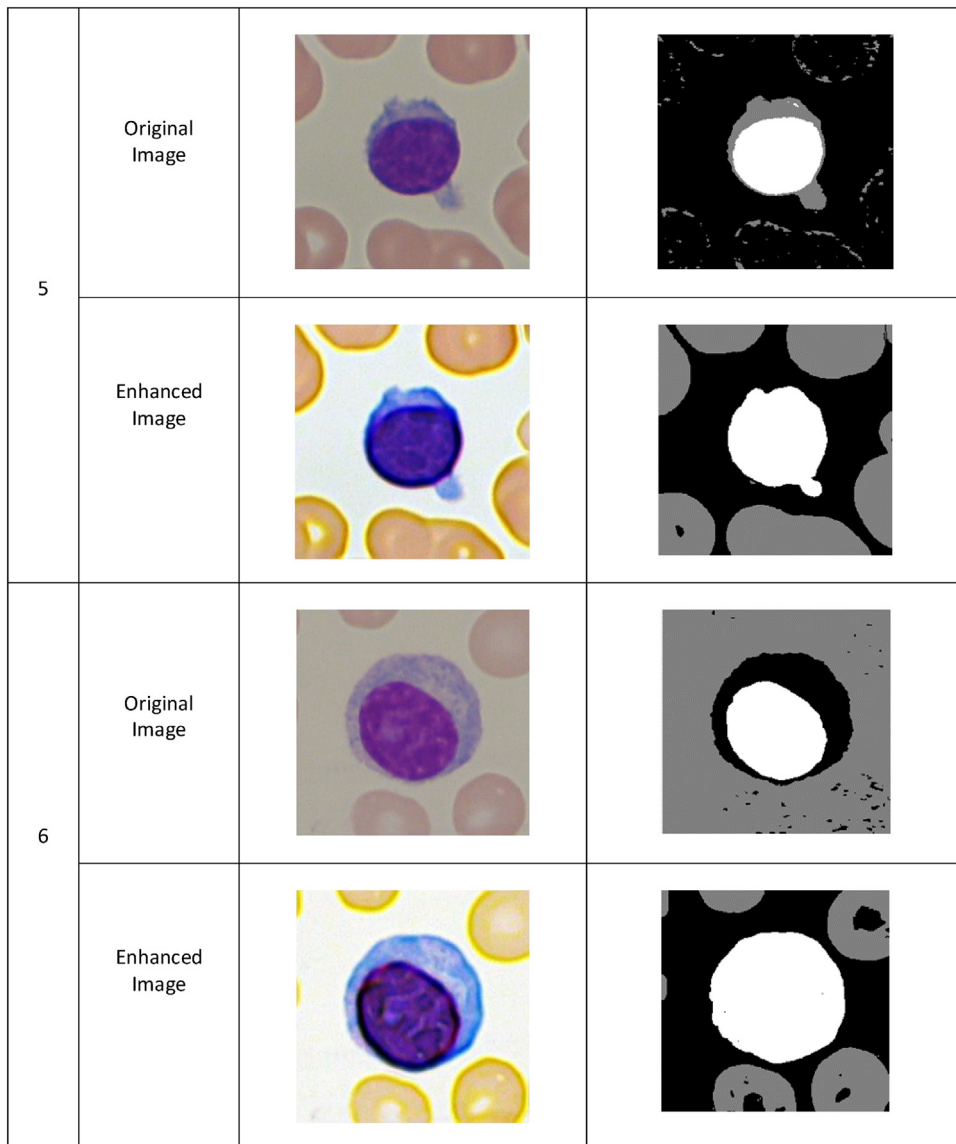


Fig. 11. (Continued)

easier. From experimental results, we observed that the image quality and its color appearance enhancement using the proposed method based on NSS are improved efficiently. Our proposed method is promising for stained pathology color image enhancement. In the future work, we plan to apply this procedure in the segmentation of blood components of the pathology images. The processing in high resolution color image under multi-criteria requires more processing time which needs to optimization and acceleration.

References

- [1] M.N. Gurcan, L. Boucheron, A. Can, A. Madabhushi, N. Rajpoot, B. Yener, Histopathological image analysis: a review, *IEEE Rev. Biomed. Eng.* 2 (2009) 147–171.
- [2] G. Musumeci, Past, present and future: overview on histology and histopathology, *J. Histol. Histopathol.* 88 (2014) 1–5.
- [3] K. Kuru, Optimization and enhancement of H&E stained microscopical images by applying bilinear interpolation method on lab color mode, *Theor. Biol. Med. Model.* 11 (9) (2014) 1742–4682.
- [4] T. Peter, K. Fu-Jen, *Optical Imaging and Microscopy. Techniques and Advanced Systems*, Springer series in optical sciences, Springer, 2008.
- [5] W.G. Gary, Connection 2010. [Online]. Available: http://www.dako.com/28829_2010.conn14.h.e.staining.oversights.insights.gill.pdf (Accessed 2 January 2016).
- [6] C. Zhang, X. Xiao, X. Li, Y. Chen, W. Zhen, J. Chang, C. Zheng, Z. Liu, White blood cell segmentation by color-space-based K-means clustering, *Sensors* 14 (2014) 16128–16147.
- [7] J.C. Russ, M. Parry-Hill, M.W. Davidson, *Digital Image Processing. Optical Microscopy Primer*, 2007.

- [8] R.J. Walter, M.W. Berns, Computer-enhanced video microscopy: digitally processed microscope images can be produced in real time, *Proc. Natl. Acad. Sci. U. S. A.* 78 (11) (1981) 6927–6931.
- [9] R.C. Gonzalez, R.E. Woods, Boston, MA, USA, in: *Digital Image Processing*, 2nd ed., Addison-Wesley Longman Publishing Co., 2001.
- [10] S.M. Pizer, E.P. Amburn, J.D. Austin, Adaptive histogram equalization and its variations, *Comput. Vis. Graphics Image Process.* 39 (1987) 355–368.
- [11] W. Chen, X. Mao, H. Ma, Low-contrast microscopic image enhancement based on multi-technology fusion, in: *Intelligent Computing and Intelligent Systems (ICIS)*, 2010 IEEE International Conference, 2010.
- [12] H. Garud, Brightness preserving contrast enhancement in digital pathology, Himachal Pradesh, Image Information Processing (ICIIP), 2011 International Conference (2011).
- [13] Z. Liu, J. Liu, X. Xiao, H. Yuan, X. Li, J. Chang, C. Zheng, Segmentation of white blood cells through nucleus mark watershed operations and mean shift clustering, *Sensors* 15 (2015) 22561–22586.
- [14] E. Reinhard, M. Adhikhmin, B. Gooch, P. Shirley, Color transfer between images, *IEEE Comput. Graphics Appl.* 21 (5) (2001) 34–41.
- [15] E.A. Mohamed, New approach for enhancing image retrieval using neutrosophic sets, *Int. J. Comput. Appl.* 95 (8) (2014) 0975–8887.
- [16] Y. Guo, A. Şengürb, J.A. Yec, Novel image thresholding algorithm based on neutrosophic similarity score, *Measurement* 58 (2014) 175–186.
- [17] Y. Guo, A. Şengürb, A novel image edge detection algorithm based on neutrosophic, *Comput. Electr. Eng.* 40 (8) (2014) 3–25.
- [18] Y. Guo, A. Şengürb, A novel color image segmentation approach based neutrosophic set and modified fuzzy c –means, *Circuits Syst. Signal. Process.* 32 (2013) 1699–1723.
- [19] B. Yu, Z. Niu, Z. Wang, Mean shift based clustering of neutrosophic domain for unsupervised constructions detection, *Optik* 124 (2013) 4697–4706.
- [20] J. Ye, Multicriteria decision-making method using the correlation coefficient under single-valued neutrosophic environment, *Int. J. Gen. Syst.* 42 (4) (2013) 386–394.
- [21] K.M. Amin, A. Shahin, Y. Guo, A novel breast tumor classification algorithm using neutrosophic score features, *Measurement* 81 (2016) 210–220.
- [22] F. Scotti, Robust segmentation and measurements techniques of white cells in blood microscope images, Sorrento, Italy, IMTC 2006—Instrumentation and Measurement (2006).
- [23] R.D. Labati, V. Piuri, F. Scotti, ALL-IDB: the acute lymphoblastic leukemia image database for image processing, in: *Image Processing (ICIP)*, 2011 18th IEEE International Conference, 2011.
- [24] L. Putzu, C. Ruberto, White blood cells identification and counting from microscopic blood image, *Int. J. Med. Health Biomed. Bioeng. Pharm. Eng.* 7 (1) (2013).
- [25] M.M. Mohamed, A framework for automatic white blood cell differential counting targeting a low cost system, *Electr. Comput. Eng.* (2012).
- [26] M. Mohamed, B. Far, A. Guaily, An efficient technique for white blood cells nuclei automatic segmentation, Seoul, IEEE International Conference on Systems and Cybernetics (SMC2012) (2012).
- [27] M.M.A. Mohamed, smartlabsltd, [Online]. Available: <http://smartlabsltd.com/Researches> (Accessed 3 January 2016).
- [28] H.L. Tan, Z. Li, Y.H. Tan, S. Rahardja, A perceptually relevant MSE-based image quality metric, *IEEE Trans. Image Process.* (2013) 4447–4459.
- [29] S. Rahman, M.M. Rahman, K. Hussain, S.M. Khaled, Image enhancement in spatial domain: a comprehensive study, Dhaka, 2014 17th International Conference on Computer and Information Technology (ICCIT) (2014).
- [30] P. Rajavel, Image dependent brightness preserving histogram equalization, *IEEE Trans. Consum. Electron.* 56 (2) (2010) 756–763.
- [31] P. Mohammadi, A.E. Moghadam, S. Shirani arxiv [Online]. Available: www.arxiv.org/pdf/1406.7799 (Accessed 20 January 2016).
- [32] H. Garud, D. Sheet, A. Suveer, P. KrishnaKarri, A.K. Ray, M. Mahadevappa, J. Chatterjee, Brightness preserving contrast enhancement in digital pathology, Himachal Pradesh, International Conference on Image Information Processing (ICIIP 2011) (2011).
- [33] J. Ping, L. Hua, X. Wu, H. Yang, Z. Zhou, Color medical image enhancement based on adaptive equalization of intensity numbers matrix histogram, *Int. J. Autom. Comput.* 12 (5) (2015) 551–558.
- [34] P. Shrestha, R. Kneepkens, G. Elswijk, J. Vrijnsen, R. Ion, D. Verhagen, E. Abels, D. Vossen, B. Hulsken, Objective and subjective assessment of digital pathology image quality, *AIMS Med. Sci.* 2 (1) (2015) 65–78.
- [35] D. Tzeng, Spectral-Based Color Separation Algorithm Development for Multiple-Ink Color, Rochester Institute of Technology, Rochester, NY, 1999.
- [36] B. Gupta, M. Tiwari, Minimum mean brightness error contrast enhancement of color images using adaptive gamma correction with color preserving framework, *Optik* 127 (2016) 671–1676.
- [37] *Blue Histology—Blood, School of Anatomy and Human Biology, The University of Western Australia, 2016 [Online]. Available: <http://www.lab.anhb.uwa.edu.au/mb140/corepages/blood/blood.htm> (Accessed 3 January 2016).